Available online at www.sciencedirect.com
SCIENCE DIRECT®
PERGAMON
International Journal of Heat and Mass Transfer 46 (2003) 1693–1701
International Journal of HEAT and MASS TRANSFER
www.elsevier.com/locate/ijhmt

Fitting the duct to the "body" of the convective flow

Tunde Bello-Ochende, Adrian Bejan *

Department of Mechanical Engineering and Materials Science, Duke University, Box 90300, Durham, NC 27708-0300, USA

Received 17 September 2002; received in revised form 25 November 2002

Abstract

This paper is a proposal to design flow structures with maximal heat transfer rate per unit volume, by shaping each duct so that it fits optimally on the body of the convective flow. Optimally shaped ducts can be assembled into larger constructs. Two examples are given. In the first, a heat-generating strip is cooled inside a duct of rectangular cross-section. The duct geometry has two degrees of freedom, which can be selected so that the fixed duct volume packs a maximum of heat transfer rate. In the second example, the duct is a tube with isothermal internal surface, and the flow is sufficiently slow so that boundary layers do not form inside the duct. Once again, the duct aspect ratio can be optimized for maximal heat transfer rate density. Further improvements can be sought by endowing the duct geometry with more degrees of freedom.

Keywords: Constructal design; Optimal duct shape; Convection; Heat transfer density; Bejan number

1. The constructal design method

The traditional approach to the design of convective flow structures such as heat exchangers and electronics cooling, starts with the channels and the ducts. Flow channels and wall features (e.g., fins) are first assumed. Later, they are connected and assembled into larger constructs that fill the space allocated to the device. The flows, which are many and highly diverse, are forced to reside in regular spaces that have been set aside for fluid flow and convection.

The traditional approach is so common that we do not even think of questioning it. The very teaching of heat transfer begins with assumed 'typical' configurations that confine convective flows: flat plates, tubes, parallel-plates channels, etc.

In this paper, we propose an alternative to this approach. The reason is the objective that drives most of the convective design activity, namely, the maximization of heat transfer rate density. Compact and small-scale heat exchangers, as well as all the electronics cooling configurations developed so far, point in the same direction: the installation of more heat transfer rate into devices the volumes of which are constrained.

This permanent struggle between objective and constraints invites us to consider alternatives. In the present paper, the guide is the method of constructal design [1], which is the thought that the flow architecture itself is the product of this struggle, or the means (the mechanism) by which the device achieves its objective under constraints. In constructal design the flow architecture is the unknown. The flow system is initially a black box endowed with objective, constraints and, above all, freedom. The freedom to morph, to go with the flow, to shape itself, to rock the boat the least.

Sadi Carnot's teachings to avoid friction and shocks (abrupt changes) in the pursuit of thermodynamic ideality (reversibility) are consistent with the constructal method. The difference is that in constructal design the finiteness of space, residence times and materials is recognized as reality. The constraints relegate the flow system to a life of thermodynamic imperfection. The system is destined to rely on flows that overcome resistances. Streams and resistances together represent irreversibility, or the degrading of thermodynamic performance at the global level. Fluid and thermal resistances cannot be

* Corresponding author. Tel.: +1-919-660-5309; fax: +1-919-660-8963.
E-mail address: dalford@duke.edu (A. Bejan).

0017-9310/03/$ - see front matter
doi:10.1016/S0017-9310(02)00477-5

Nomenclature

A	duct cross-sectional area, m^2
Be	Bejan number based on volume, Eq. (12)
Be_L	Bejan number based on L, Eq. (21)
D	thickness, m
G	width, m
H	height, m
k	thermal conductivity, W/mK
L	length, m
L_d	downstream flow length, m
L_u	upstream flow length, m
P	pressure, Pa
Pr	Prandtl number, ν/α
q	total heat transfer, W
q''	heat flux, W/m^2K
Q	dimensionless heat transfer density, Eq. (16)
R	radius, m
R_∞	radius of computational domain, m
Re	Reynolds number, Eq. (31)
T	temperature, K
T_w	wall temperature, K
T_0	inlet temperature, K
u, v, w	velocity components, m/s
V	duct volume, m^3
x, y, z	Cartesian coordinates, m

Greek symbols

α	thermal diffusivity, m^2/s
ΔP	pressure difference, Pa
μ	viscosity, kg/sm
ν	kinematic viscosity, m^2/s
ρ	density, kg/m^3

Subscripts

m	maximum
mm	maximized twice
opt	optimum
w	wall

Superscript

(˜)	dimensionless variables, Eqs. (9), (29) and (30)

eliminated. At best, they can be shaped, distributed and balanced against each other, so that their integrated (global) effect is minimized. The end result of such morphological changes is the flow architecture of the system.

Let us reexamine the traditional approach mentioned in the first paragraph. To force a flow to perform inside a standard, prescribed geometry is like forcing your foot into a standard (one-size) shoe. You may be able to walk, but you will soon think of better alternatives. The flow, like the foot, has its own "body". For example, the body of the thermally convective flow near a flat plate parallel to a stream is the thermal boundary layer region. This body has a natural shape. Our proposal is general: start with the body, and build the confining walls so that they mate with the body as well as possible. The foot comes before the shoe.

To illustrate this approach, consider the problem of cooling a heat-generating line (or narrow strip) with a stream that flows parallel to the strip (Fig. 1, top). The global objective is to fit this convective flow into the smallest volume, or to pack the largest heat transfer rate in a volume of fixed size and variable shape. The natural body of the convective flow can be anticipated based on boundary layer theory. As shown in Fig. 1, we expect a convective region shaped as a body of revolution, which becomes thicker in the downstream direction.

Next comes the task of shaping the volume so that it mimics the geometry of the convective body. The ideal way to proceed is to give the fixed volume V a large number of degrees of freedom, and to optimize the heat transfer rate density with respect to each degree. The simplest version of this approach is to endow the volume V with a single degree of freedom, so that we still have access to an infinity of V shapes that could be fitted around the convective body.

In Fig. 1, it was assumed that V is a cylinder positioned coaxially with the heat strip, and that the slenderness of the cylinder is free to vary. Three competing designs are shown. When the shape of V is robust, Fig. 1a, a large portion of V is wasted because it is bathed by fluid that does not "work". The isothermal fluid that is outside the convective body is useless. In the opposite extreme, Fig. 1c, the V shape is considerably more slender than the convective body, and the heat-transfer fluid is "overworked". Most of the downstream position of the heat-generating strip is cooled by fluid that has been used already. The stream warms up as it flows downstream, and becomes a poorer cooling agent.

The best V shape is in-between, Fig. 1b. An enclosure that hugs the contour of the convective body promises to be filled to the maximum with cold fluid that interacts thermally with the heat source. In this paper, we investigate this design optimization opportunity numerically.

2. Heating strip inside duct

The first demonstration of the duct-fitting principle is for the test configuration shown in Fig. 2. A thin heat-generating strip of width 2D and temperature T_w is bathed on one side by a single-phase stream of temperature T_0.

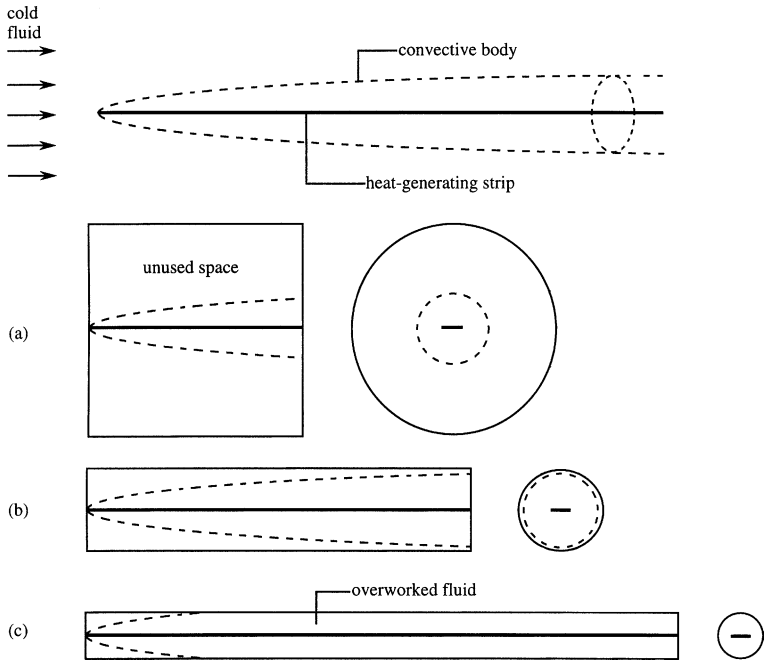

Fig. 1. The body of a convective flow, and how to fit a duct around it.

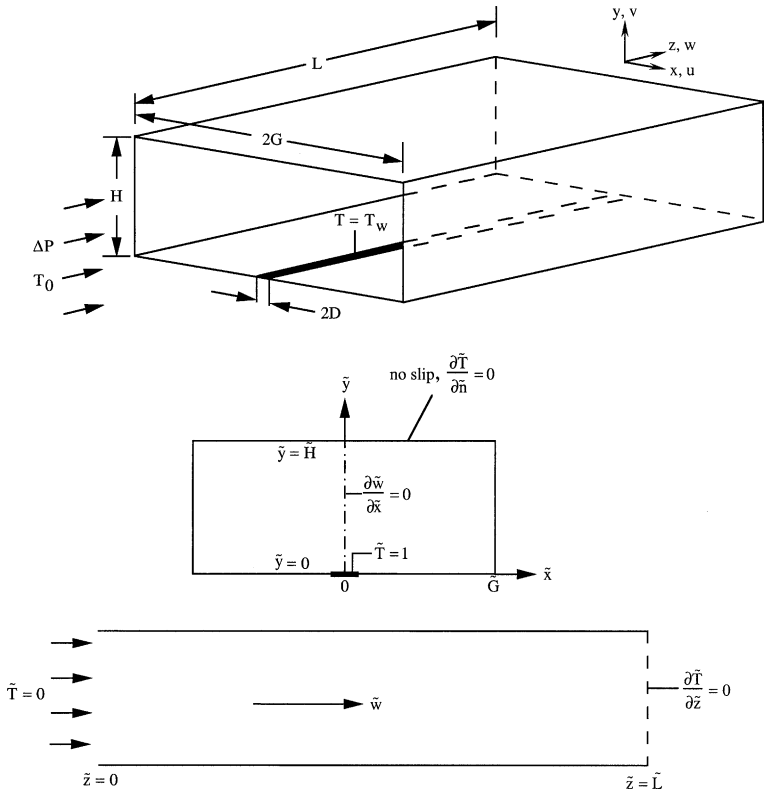

Fig. 2. Heat-generating strip cooled by a parallel stream, and encased in a duct of fixed volume and variable shape.

A related flow geometry was analyzed numerically in [2]. This time the objective is to encase the flow in a duct with variable shape and fixed volume, such that the volume-averaged heat transfer rate density is maximized. This optimum corresponds to the situation sketched in Fig. 1b, where the given volume is filled to the maximum with flow that participates in the heat transfer process. The symmetry of the configuration allows us to study only half of the flow volume, which serves as constraint

$$V = GHL \tag{1}$$

The pressure difference that drives the flow, ΔP, is specified. The flow is steady and laminar. The equations for the conservation of mass, momentum and energy are

$$\frac{\partial u}{\partial x}+\frac{\partial v}{\partial y}+\frac{\partial w}{\partial z}=0 \tag{2}$$

$$u\frac{\partial u}{\partial x}+v\frac{\partial u}{\partial y}+w\frac{\partial w}{\partial z}=-\frac{1}{\rho}\frac{\partial P}{\partial x}+\nu\left(\frac{\partial^2 u}{\partial x^2}+\frac{\partial^2 u}{\partial y^2}+\frac{\partial^2 u}{\partial z^2}\right) \tag{3}$$

$$u\frac{\partial v}{\partial x}+v\frac{\partial v}{\partial y}+w\frac{\partial v}{\partial z}=-\frac{1}{\rho}\frac{\partial P}{\partial y}+\nu\left(\frac{\partial^2 v}{\partial x^2}+\frac{\partial^2 v}{\partial y^2}+\frac{\partial^2 v}{\partial z^2}\right) \tag{4}$$

$$u\frac{\partial w}{\partial x}+v\frac{\partial w}{\partial y}+w\frac{\partial w}{\partial z}=-\frac{1}{\rho}\frac{\partial P}{\partial z}+\nu\left(\frac{\partial^2 w}{\partial x^2}+\frac{\partial^2 w}{\partial y^2}+\frac{\partial^2 w}{\partial z^2}\right) \tag{5}$$

$$u\frac{\partial T}{\partial x}+v\frac{\partial T}{\partial y}+w\frac{\partial T}{\partial z}=\alpha\left(\frac{\partial^2 T}{\partial x^2}+\frac{\partial^2 T}{\partial y^2}+\frac{\partial^2 T}{\partial x^2}\right) \tag{6}$$

where u, v and w are the velocity components in the x, y and z directions, and z is aligned with the flow direction. The fluid properties (α, ν, ρ) are defined in the Nomenclature, and are assumed constant. The local pressure and temperature are P and T.

First, Eqs. (3)–(5) can be simplified by assuming that the effect of inertia is negligible. This is equivalent to the assumption that the fluid Prandtl number is greater than 1. In this limit the flow is hydrodynamically fully developed, and the momentum equations reduce to a single equation

$$\left(\frac{\partial^2 w}{\partial x^2}+\frac{\partial^2 w}{\partial y^2}\right)=\frac{\Delta P}{\mu L} \tag{7}$$

The energy equation becomes

$$w\frac{\partial T}{\partial z}=\alpha\left(\frac{\partial^2 T}{\partial x^2}+\frac{\partial^2 T}{\partial y^2}+\frac{\partial^2 T}{\partial z^2}\right) \tag{8}$$

The boundary conditions are $w=0$ on all the wall surfaces, zero shear on the plane of symmetry ($x=0$), $T=T_w$ on the heat-generating strip, $T=T_0$ on the inlet plane, and zero heat flux on the wall surfaces other than the heat generating strip. As the boundary condition for temperature on the exit plane ($z=L$) we use the parabolic condition $\partial T/\partial z=0$.

Eqs. (7) and (8) are nondimensionalized by using $V^{1/3}$ as length scale and T_w-T_0 as temperature scale,

$$(\tilde{x},\tilde{y},\tilde{z},\widetilde{H},\widetilde{G},\widetilde{L},\widetilde{D})=\left(\frac{x,y,z,H,G,L,D}{V^{1/3}}\right),$$
$$\widetilde{T}=\frac{T-T_0}{T_w-T_0},\quad \tilde{w}=\frac{w\mu}{\Delta P V^{1/3}} \tag{9}$$

Eqs. (7) and (8) become

$$\frac{\partial^2\tilde{w}}{\partial\tilde{x}^2}+\frac{\partial^2\tilde{w}}{\partial\tilde{y}^2}=\frac{1}{\widetilde{L}} \tag{10}$$

$$\tilde{w}Be\frac{\partial\widetilde{T}}{\partial\tilde{z}}=\frac{\partial^2 T}{\partial x^2}+\frac{\partial^2\widetilde{T}}{\partial\tilde{y}^2}+\frac{\partial^2\widetilde{T}}{\partial\tilde{z}^2} \tag{11}$$

where

$$Be=\frac{\Delta P V^{2/3}}{\alpha\mu} \tag{12}$$

The dimensionless group Be is the dimensionless pressure drop that Bhattacharjee and Grosshandler [3] and Petrescu [4] named the Bejan number. This number is fixed because ΔP and V are fixed. The volume constraint (1) becomes

$$\widetilde{H}\widetilde{G}\widetilde{L}=1 \tag{13}$$

The temperature boundary conditions are $\widetilde{T}=1$ on the strip, $\partial\widetilde{T}/\partial\tilde{n}=0$ on the other wall surfaces, $\widetilde{T}=0$ on the plane of the inlet, and $\partial\widetilde{T}/\partial\tilde{z}=0$ on the plane of the outlet.

The global quantity that measures the goodness of the duct design is the heat transfer rate density, i.e., the heat transfer rate that occurs in the entire volume. The total heat transfer rate from the strip to the fluid is

$$q=\int_0^L\int_0^D q''\,\mathrm{d}x\,\mathrm{d}z \tag{14}$$

where q'' is the local heat flux along the D-wide surface of the strip,

$$q''=k\left(-\frac{\partial T}{\partial y}\right)_{y=0} \tag{15}$$

The heat transfer rate density q/V has the dimensionless counterpart

$$Q=\frac{q/V}{k(T_w-T_0)/V^{2/3}}=\int_0^{\widetilde{L}}\int_0^{\widetilde{D}}\left(-\frac{\partial\widetilde{T}}{\partial\tilde{y}}\right)_{\tilde{y}=0}\mathrm{d}\tilde{x}\,\mathrm{d}\tilde{z} \tag{16}$$

3. Numerical optimization of duct geometry

Eqs. (10) and (11) were solved based on the finite element method. First, the velocity distribution $\tilde{w}(\tilde{x},\tilde{y})$

Table 1
Grid refinement test for $\widetilde{L} = 9.5$, $H/G = 1.3$ and $Be = 10^5$

Nodes	Elements	Q	$\lvert(Q^i - Q^{i+1})/Q^i\rvert$
7000	8123	2.5399	–
12,375	14,192	2.5838	0.0173
24,750	28,292	2.5957	0.0046
49,500	56,492	2.60374	0.0031

was obtained by solving Eq. (10). Next, the temperature field $\widetilde{T}(\tilde{x}, \tilde{y}, \tilde{z})$ followed directly from Eq. (11). The finite element code [5] was selected because in order to optimize the geometry of the flow enclosure it was necessary to simulate the flow in a very large number of configurations. The grids were nonuniform in the $\tilde{x}$, $\tilde{y}$ and $\tilde{z}$ directions, and changed from one configuration to the next. The nodes were denser in the vicinity of the strip, where higher temperature gradients were expected. The total number of nodes was in the range 9600–108,000. The total number of elements varied from 10,773 to 139,499. The meshes that were used were tested so that the doubling of the number of nodes in the $\tilde{x}$, $\tilde{y}$ and $\tilde{z}$ directions induced changes of less than 2% in Q. Table 1 shows one example of how grid independence was achieved. In this example, i indicates the grid, and increases downward through the table.

The strip half-width was set at a value in the range $0.0025 \leqslant \widetilde{D} \leqslant 0.02$. The pressure drop number was assigned a value in the range $1 \leqslant Be \leqslant 10^6$. The optimization of the shape of the duct volume has two degrees of freedom, $\widetilde{L}$ and the aspect ratio $\widetilde{H}/\widetilde{G}$, or H/G. These were optimized together, in two nested loops. First, in the inner loop we fixed $\widetilde{L}$ and optimized H/G, as shown in Fig. 3. The results of this first step are the aspect ratio $(H/G)_{\text{opt}}$ and the maximized heat transfer rate density Q_{m}. In the outer loop, we maximized Q_{m} by varying $\widetilde{L}$, as shown in Fig. 4.

The results of this procedure are the optimized geometry, $\widetilde{L}_{\text{opt}}$ and $(H/G)_{\text{opt}}$, and the maximal heat transfer rate density, Q_{mm}, which is the largest of the Q_{m} values. These results are functions of the assumed parameters, Be and $\widetilde{D}$. Fig. 5 was generated by repeating the procedure of Figs. 3 and 4 for several values of Be and $\widetilde{D}$. The strip width has almost no effect on the optimized geometry, because D is small relative to the length scale of the flow enclosure, $V^{1/3}$. The maximized heat transfer rate density Q_{mm} increases as the strip becomes wider.

The effect of the pressure drop number is more interesting. Two patterns of behavior emerge. When $Be > 10^2$, Q_{mm} and $\widetilde{L}_{\text{opt}}$ increase with Be, and $(H/G)_{\text{opt}}$ is practically constant, $(H/G)_{\text{opt}} \cong 1.33$. The optimal cross-sectional shape is almost square. In the large-Be limit, and if $\widetilde{D} = 0.02$, the remaining results vary as

$$\widetilde{L}_{\text{opt}} \cong 0.5Be^{1/4} \tag{17}$$

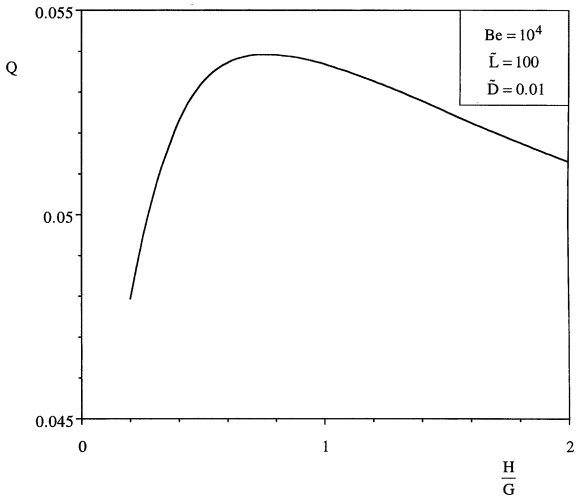

Fig. 3. The optimization of the duct cross-sectional shape when the duct length is fixed ($\widetilde{L} = 10^2$, $\widetilde{D} = 10^{-2}$, $Be = 10^4$).

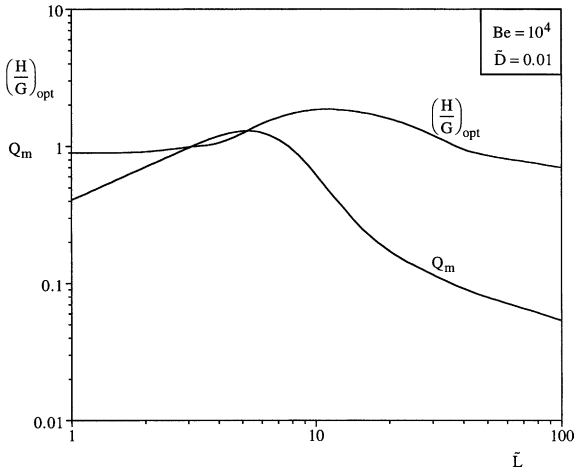

Fig. 4. Optimization of results of the type shown in Fig. 3, repeated for many values of $\widetilde{L}$.

$$Q_{\text{mm}} \cong 0.194Be^{1/4} \tag{18}$$

In view of $(H/G)_{\text{opt}} \cong 1.33$ and the volume constraint (13), the optimized length shown in Eq. (17) is equivalent to an optimal slenderness of the longitudinal profile,

$$\left(\frac{L}{H}\right)_{\text{opt}} \cong 0.31Be^{3/8} \tag{19}$$

Furthermore, by eliminating V between Eqs. (17) and (19), the slenderness of the flow enclosure becomes

$$\left(\frac{L}{H}\right)_{\text{opt}} \cong 0.43Be_L^{1/4} \tag{20}$$

where Be_L is the Bejan number based on L [6],

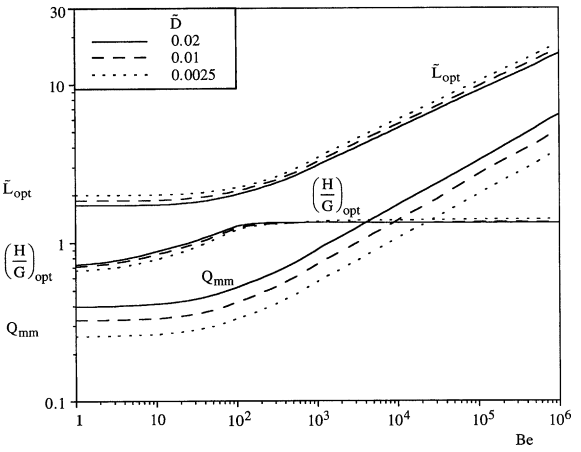

Fig. 5. The effect of pressure drop number and strip width on the optimized duct that houses the convective flow of Fig. 2.

$$Be_L = \frac{\Delta P L^2}{\alpha \mu} \tag{21}$$

Note the similarities between the Be_L and Be definitions, Eqs. (21) and (12), and that the length scale used in Be is $V^{1/3}$. Eq. (17) is the same as writing

$$Be_L^{1/2} \cong 0.5 Be^{3/4} \tag{22}$$

Note further that Eq. (20) has the same form as the relation obtained for the optimal slenderness of spacings in large stacks of parallel plates with convective heat transfer and fixed volume and longitudinal pressure drop [6]. Additional examples of optimized spacings are reviewed in [7]. When the flow is laminar ($Pr \gtrsim 0.5$) and driven by buoyancy through a stack with many vertical channels, the optimal spacing (H) is given by a relation similar to Eq. (20), where L is the height of the stack, and Be_L is replaced by the Rayleigh number based on height [8–10]. More examples of optimal internal spacings for structures with many vertical channels cooled by natural convection are given in [7].

When $Be < 10^2$, the $\widetilde{L}_{\text{opt}}$ and Q_{mm} curves level off, and $(H/G)_{\text{opt}}$ drops to almost half of its original value. This behavior requires closer scrutiny, because when Be decreases the flow slows down and the thermal boundary layers become thicker. The convective body formed around the heating strip becomes less slender, and, because the volume is constrained, the $(L/H)_{\text{opt}}$ ratio decreases. This ratio has to remain greater than 1 in an order of magnitude sense, say

$$\left(\frac{L}{H}\right)_{\text{opt}} > 10 \tag{23}$$

so that the model adopted in Fig. 2 is adequate. By this we mean that the volume must be sufficiently slender so that the $Pr \gg 1$ flow can attain full development, and the upstream and downstream flow regions (the entrance and exit effects) can be neglected in the calculation of the overall ΔP. In sum, by combining Eqs. (20)–(23) we find that the slenderness assumption (23) is the same as

$$Be > 10^4 \tag{24}$$

This condition suggests that the small-Be behavior shown in Fig. 5 may be due to the breakdown of the slender channel model. This is why in the next section we built a model more suitable for volume shapes and slow flows that violate the inequality (23).

4. Round tube with upstream and downstream flow

To account for the flow upstream and downstream of a duct that is not necessarily slender, we chose the short tube configuration shown in Fig. 6. The flow, pressure and temperature fields (u, v, P, T) depend on the radial and longitudinal positions (r,x). These variables are defined in Fig. 6. The tube length and radius are L and R. The computational domain is considerably larger than the tube volume: it has the radius R_∞ and the length $L_u + L + L_d$, where L_u and L_d are the lengths of the upstream and downstream flow regions. The dimensions R_∞, L_u and L_d are chosen to be sufficiently larger than R and L, so that their magnitudes do not affect the calculated pressure drop (ΔP) and total heat transfer rate associated with the tube. To preserve cylindrical symmetry, the tube wall is assumed isothermal (T_w).

The equations for the conservation of mass, momentum and energy in steady flow are

$$\frac{1}{\tilde{r}}\frac{\partial(\tilde{r}\tilde{v})}{\partial \tilde{r}} + \frac{\partial \tilde{u}}{\partial \tilde{x}} = 0 \tag{25}$$

$$\tilde{v}\frac{\partial \tilde{v}}{\partial \tilde{r}} + \tilde{u}\frac{\partial \tilde{v}}{\partial \tilde{x}} = -\frac{\partial \widetilde{P}}{\partial \tilde{r}} + \frac{1}{Re}\left(\frac{\partial^2 \tilde{v}}{\partial \tilde{r}^2} + \frac{1}{\tilde{r}}\frac{\partial \tilde{v}}{\partial \tilde{r}} - \frac{\tilde{v}}{\tilde{r}^2} + \frac{\partial^2 \tilde{v}}{\partial \tilde{x}^2}\right) \tag{26}$$

$$\tilde{v}\frac{\partial \tilde{u}}{\partial \tilde{r}} + \tilde{u}\frac{\partial \tilde{u}}{\partial \tilde{x}} = -\frac{\partial \widetilde{P}}{\partial \tilde{x}} + \frac{1}{Re}\left(\frac{\partial^2 \tilde{u}}{\partial \tilde{r}^2} + \frac{1}{\tilde{r}}\frac{\partial \tilde{u}}{\partial \tilde{r}} + \frac{\partial^2 \tilde{u}}{\partial \tilde{x}^2}\right) \tag{27}$$

$$\tilde{v}\frac{\partial \widetilde{T}}{\partial \tilde{r}} + \tilde{u}\frac{\partial \widetilde{T}}{\partial \tilde{x}} = \frac{1}{RePr}\left[\frac{1}{\tilde{r}}\frac{\partial}{\partial \tilde{r}}\left(\tilde{r}\frac{\partial \widetilde{T}}{\partial \tilde{r}}\right) + \frac{\partial^2 \widetilde{T}}{\partial \tilde{x}^2}\right] \tag{28}$$

The dimensionless variables are defined based on the length scale $V^{1/3}$, where V is the tube volume, and the pressure difference between the inlet and exit planes of the computational domains (ΔP),

$$(\tilde{r},\tilde{x},\widetilde{R},\widetilde{R}_\infty,\widetilde{L},\widetilde{L}_u,\widetilde{L}_d) = (r,x,R,R_\infty,L,L_u,L_d)/V^{1/3} \tag{29}$$

$$(\tilde{u},\tilde{v}) = \frac{(u,v)}{(\Delta P/\rho)^{1/2}} \quad \widetilde{P} = \frac{P - P_d}{\Delta P} \tag{30}$$

The temperature $\widetilde{T}$ is defined as in Eq. (9). The pressure on the exit plane is P_d. The Reynolds number is defined by

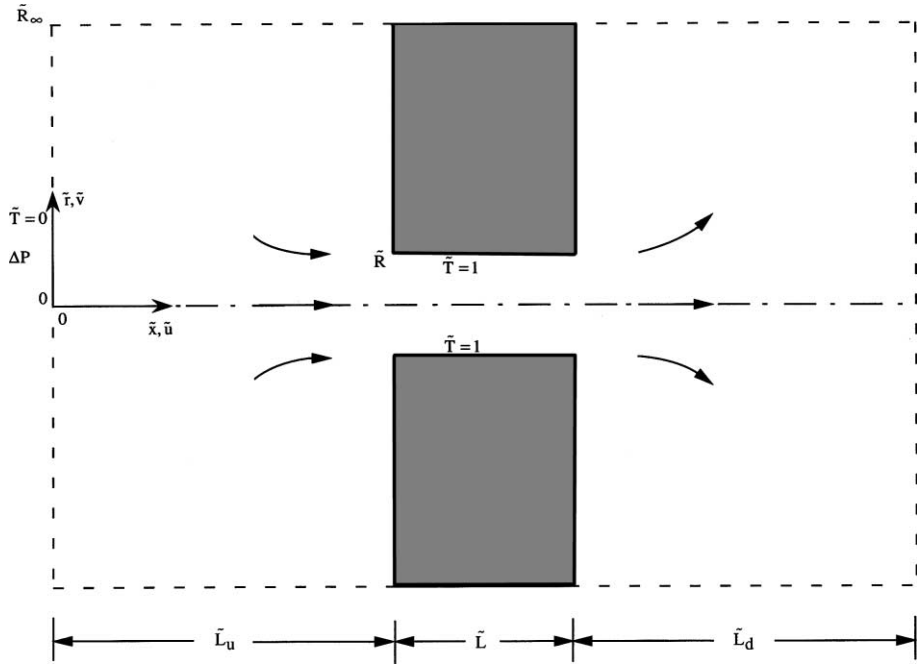

Fig. 6. Computational domain for flow through a round tube.

$$Re = \frac{V^{1/3}}{\nu}\left(\frac{\Delta P}{\rho}\right)^{1/2} = \left(\frac{Be}{Pr}\right)^{1/2} \tag{31}$$

The boundary conditions for fluid flow are: $\widetilde{P}=1$ and $\tilde{v}=0$ on the left-most plane ($\tilde{x}=0$); $\widetilde{P}=0$ on the right-most plane ($\tilde{x}=\widetilde{L}_u+\widetilde{L}+\widetilde{L}_d$); no slip and no flow penetration on all the solid surfaces; and free slip and no flow penetration at $\tilde{r}=0$ and $\tilde{r}=\widetilde{R}_\infty$.

The thermal boundary conditions are: $\widetilde{T}=1$ on the internal surface of the tube; $\widetilde{T}=0$ on the $\tilde{x}=0$ plane; adiabatic surfaces on the remaining portions of the boundary of the computational domain.

The quantity that describes the global performance of the flow configuration is the *density* of heat transfer, defined in dimensionless form in Eq. (16). The tube volume is fixed, $\pi\widetilde{R}^2\widetilde{L}=1$, while the volume shape may vary. The variable shape is represented by $\widetilde{R}$, or $\widetilde{L}$.

Eqs. (25)–(28) were solved using a finite elements code [7]. The grid was nonuniform in $\tilde{x}$ and $\tilde{r}$, with more nodes on the tube surface and in the vicinity of the tube entrance and exit. Tests similar to Table 1 indicated that the number of nodes required to achieve grid independence varied from 193 to 217 nodes in the $\tilde{x}$ direction, and from 129 to 147 nodes in the $\tilde{r}$ direction. With such grids, the numerical solution showed relative changes of less than 2% when the number of grid points was doubled in both directions.

The outer dimensions of the computational domain ($\widetilde{L}_u$, $\widetilde{L}_d$, $\widetilde{R}_\infty$) were selected based on the tests documented in Tables 2 and 3. These lengths were made large enough so that the relative changes in the heat transfer rate density became smaller than 1%. The outer dimensions selected and used to generate Fig. 7 were $\widetilde{L}_u=20$, $\widetilde{L}_d=20$ and $\widetilde{R}_\infty=20+\widetilde{R}$. For Fig. 8, the outer dimension varies and depends on Be; $\widetilde{L}_u$ is equal to $\widetilde{L}_d$ and varies from 12 to 22; $\widetilde{R}_\infty$ varies from 14 to 24.3.

Table 2
Test for determining the outer dimensions of the computational domain ($\widetilde{R}=2$, $Be=0.01$)

$\widetilde{L}_u$	L_d	$\widetilde{R}_\infty=\widetilde{L}_u+\widetilde{R}$	Q	$\lvert(Q^i-Q^{i+1})/Q^i\rvert$
2	2	4	4.310311	–
4	4	6	3.502901	0.18732
6	6	8	3.203732	0.085406
8	8	10	3.044779	0.049615
10	10	12	2.943181	0.03337
12	12	14	2.870837	0.02458
14	14	16	2.815622	0.01923
16	16	18	2.771426	0.01570
18	18	20	2.734814	0.01321
20	20	22	2.703698	0.01138
22	22	24	2.676722	0.00998
24	24	26	2.652967	0.00887

The tube geometry was optimized by simulating the flow and temperature fields for a large number of tube shapes ($\widetilde{R}$), calculating the heat transfer rate density Q for each shape, and selecting the shape for which Q is maximal. Fig. 7 confirms that Q has a maximum with respect to the shape parameter $\widetilde{L}$ when the tube volume

Table 3
Test for determining the outer dimensions of the computation domain ($\widetilde{R} = 2$, and $Be = 100$)

$\widetilde{L}_u$	L_d	$\widetilde{R}_\infty = \widetilde{L}_u + \widetilde{R}$	Q	$\lvert(Q^i - Q^{i+1})/Q^i\rvert$
2	2	4	6.583452	–
4	4	6	5.973845	0.09260
6	6	8	5.726921	0.041334
8	8	10	5.576024	0.02635
10	10	12	5.467649	0.01944
12	12	14	5.383362	0.015415
14	14	16	5.314645	0.012765
16	16	18	5.256783	0.01089
18	18	20	5.206920	0.009485
20	20	22	5.163183	0.00840

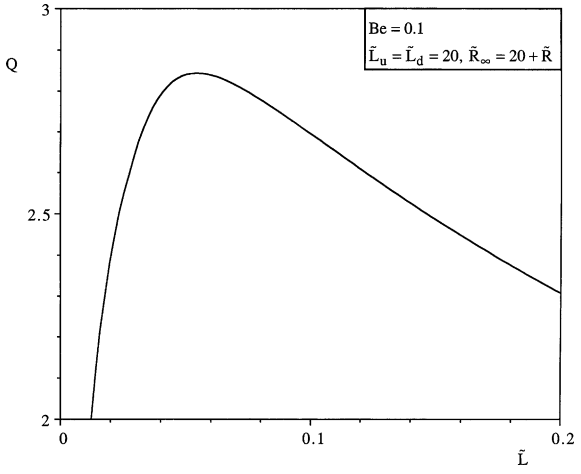

Fig. 7. The maximization of heat transfer rate density in the configuration of Fig. 6.

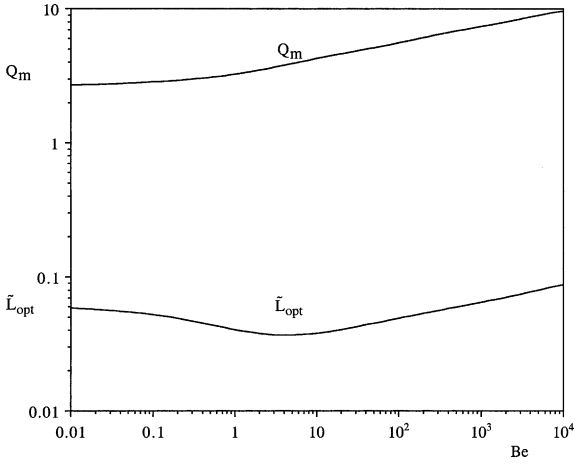

Fig. 8. The effect of pressure drop number on the optimized tube for the flow configuration simulated in accordance with Fig. 6.

is fixed. This example is for $Be = 0.1$, which is much lower than the Be range explored in Sections 2 and 3.

The optimization illustrated in Fig. 7 was repeated for several Be values in the range 10^{-2}–10^4. The maximized heat transfer density (Q_m) and optimal tube length $[\widetilde{L}_{opt} = (\pi \widetilde{R}^2_{opt})^{-1}]$ are reported in Fig. 8. This figure can be compared qualitatively with Fig. 5, which was for a flow model for slender channels, or $Be \gg 1$. Note that the Q_m and $\widetilde{L}_{opt}$ curves of Fig. 8 correspond to the Q_{mm} and $\widetilde{L}_{opt}$ curves of Fig. 5.

The present model is applicable in the limit of short tubes, or $Be \lesssim 1$. Fig. 8 confirms the features of Fig. 5 at $Be \sim 1$. As Be decreases, the maximized heat transfer density becomes less sensitive to Be. The optimal tube length shows a similar decrease in sensitivity, as Be drops below 1. The new feature is the slight dip in the $\widetilde{L}_{opt}(Be)$ curve, which occurs when Be is of order 1.

5. Concluding remarks

In this paper we provided an illustration of the method of fitting the duct to the natural shape of the convective flow. In the configuration chosen in Fig. 1 the duct had two degrees of freedom – the aspect ratio of the cross-section, and the slenderness of the longitudinal profile. In the round tube configuration of Fig. 6, the only degree of freedom was the longitudinal profile. These simple examples showed how the duct shape can be fitted to the convective body so that the volumetric density of heat transfer is maximized.

The numerical work of Section 4 made an additional contribution: the optimization of the duct profile in the slow flow limit, where the duct slenderness assumption fails. The existing studies of optimally spaced stacks of parallel plates are all based on the assumption that boundary layers and duct profiles are slender. The small-Be trends reported in Fig. 8 are new.

Better designs can be achieved by endowing the duct geometry with more degrees of freedom. In principle, this means that in addition to the optimized geometric ratios documented in this paper, a duct that houses a boundary layer flow should have a certain variation of cross-section in the longitudinal direction, most likely with wider cross-sections near the exit. Ultimately, the volume with maximal heat transfer density will be packed *nonuniformly* with flow passages and heat transfer surfaces, for example, as in dendritic constructal heat exchangers [11]. This is particularly relevant to the design of electronic packages and packed beds for energy storage and retrieval [12].

Acknowledgements

This research was supported by a grant received from the National Science Foundation.

References

[1] A. Bejan, Shape and Structure, from Engineering to Nature, Cambridge University Press, Cambridge, UK, 2000.
[2] T. Bello-Ochende, F.L. Bello-Ochende, Steady state laminar mixed convection in horizontal duct heated along the left lower semi-perimeter, Int. J. Heat Technol. 18 (2000) 53–60.
[3] S. Bhattacharjee, W.L. Grosshandler, The formation of a wall jet near a high temperature wall under microgravity environment, ASME HTD 96 (1988) 711–716.
[4] S. Petrescu, Comments on the optimal spacing of parallel plates cooled by forced convection, Int. J. Heat Mass Transfer 37 (1994) 1283.
[5] FIDAP Theory Manual v. 8.6, Fluid Dynamics International, Evanston, IL, 1998.
[6] A. Bejan, E. Sciubba, The optimal spacing for parallel plates cooled by forced convection, Int. J. Heat Mass Transfer 35 (1992) 3259–3264.
[7] S.J. Kim, S.W. Lee (Eds.), Air Cooling Technology for Electronic Equipment, CRC Press, Boca Raton, FL, 1996, Chapter 1.
[8] A. Bar-Cohen, W.M. Rohsenow, Thermally optimum spacing of vertical, natural convection cooled, parallel plates, J. Heat Transfer 106 (1984) 116–123.
[9] A. Bejan, Convection Heat Transfer, Wiley, New York, 1995, ch. 4, Problem 11, p. 157.
[10] N.K. Anand, S.H. Kim, L.S. Fletcher, The effect of plate spacing on free convection between heated parallel plates, J. Heat Transfer 114 (1992) 515–518.
[11] A. Bejan, Dendritic constructal heat exchanger with small-scale crossflows and larger-scales counterflows, Int. J. Heat Mass Transfer 45 (2002) 4607–4620.
[12] E.C. Nsofor, G.A. Adebiyi, Measurements of gas-particle convective heat transfer coefficient in a packed bed for high-temperature energy storage, Exp. Thermal Fluid Sci. 24 (2001) 1–9.